Processing and Application of Ceramics 10 [3] (2016) 153–160
DOI: 10.2298/PAC1603153S

First-principles insights on mechanical and electronic properties of TiX (X = C, N) in β-Si_3N_4 based ceramics

Harsha Varthan Shanmugakumar[1], Nagarajan Veerappan[2], Chandiramouli Ramanathan[2,*]

[1]*School of Mechanical Engineering SASTRA University, Tirumalaisamudram, Thanjavur - 613 401, India*
[2]*School of Electrical & Electronics Engineering SASTRA University, Tirumalaisamudram, Thanjavur - 613 401, India*

Received 26 May 2016; Received in revised form 26 August 2016; Accepted 12 September 2016

Abstract

The mechanical and electronic properties of β-Si_3N_4, TiC-Si_3N_4 and TiN-Si_3N_4 ceramics are investigated using density functional theory implemented with GGA/PBE functional. The pristine β-Si_3N_4 exhibits fracture for a strain of 10%. However, TiC-Si_3N_4 and TiN-Si_3N_4 ceramics exhibits fracture for a strain of 20%. The Young's modulus, shear modulus and bulk modulus of the pristine β-Si_3N_4, TiC-Si_3N_4 and TiN-Si_3N_4 ceramics are reported. TiN-Si_3N_4 ceramic is found to be the least compressible and hard. The band gap is found to decrease for TiC-Si_3N_4 and TiN-Si_3N_4 ceramics compared with the pristine β-Si_3N_4. The density of states spectrum shows more peak maxima for TiC-Si_3N_4 and TiN-Si_3N_4 ceramics rather than β-Si_3N_4. The finding of the present work gives a clear insight on the mechanical and electronic properties of β-Si_3N_4, TiC-Si_3N_4 and TiN-Si_3N_4 ceramics at the atomistic level.

Keywords: *β-Si_3N_4, ceramics, elastic constant, modulus, band gap*

I. Introduction

Silicon nitride (Si_3N_4) remains a promising material, which attracts research community in recent years owing to its excellent physical and chemical properties. Si_3N_4 exists in three predominant phases, namely α, β and γ along with other novel forms such as t-Si_3N_4, m-Si_3N_4, o-Si_3N_4 under different temperature and pressure. β-Si_3N_4 phase possesses hexagonal closed packed (HCP) crystal structure with ABAB stacking [1] and gets transformed into α-Si_3N_4 phase for the temperature of 1600 K under the applied pressure of 7.98 GPa. Besides, α-Si_3N_4 phase possesses a hexagonal crystal system with ABCDABCD stacking and gets converted into γ-Si_3N_4 phase under the pressure and temperature of 16.1 GPa and 1700 K, respectively [2]. β-Si_3N_4 can be synthesized through carbothermal reduction nitration [3], combustion synthesis [4], organic-inorganic reaction route [5], low temperature sintering [6], catalytic pyrolysis [7], partial sintering and the starch addition of Si_3N_4 powders [8]. β-Si_3N_4 proves to be a significant functional material, which has excellent mechanical properties, such as high hardness [8], good fracture toughness [8], creep resistance [8], corrosion resistance [8], wear resistance [9] and thermal shock resistance [8]. Si_3N_4 typical applications are found in many challenging areas, which include turbine blades, internal combustion engines, orthopaedic surgeries, roller mills and solar heat absorbers [10]. Moreover, in automotive industry rocker arm pads and ball bearings are prone to recurrent mechanical failure, such as fatigue, adhesion and wear, which are manufactured using Si_3N_4. Furthermore, tools for heavy machining [11] should be robust with high hardness. Thus, Si_3N_4 exhibits fracture toughness twice as that of alumina based ceramics, which enables the production engineers to use Si_3N_4 in fast machining operation on hard compounds. Moreover, silicon nitride received special attention due to its electronic properties mainly in the application as a gate dielectric in field effect transistors, as a charge storage medium in nonvolatile memories, space projects and etch mask in microelectronics. Density functional theory (DFT) method is an efficient method to study the mechanical properties of materials and to investigate the electronic structure of many body systems. The DFT method provides a user friendly ap-

*Corresponding author: tel: +91 4362 264120,
fax: +91 4362 264120, e-mail: *rcmoulii@gmail.com*

proach to probe the mechanical properties of the materials and the results from the study can be utilized in the experimental synthesis of functional materials. Duan *et al*. [12] reported the reinforcement of TiX (X = N, C) into Si_3N_4 matrix, which will inevitably result in the enhancement of mechanical properties of the material. Kargin *et al.* [13] synthesized Si_3N_4/TiN composite using TiO_2-modified Si_3N_4 powders. Maglica *et al.* [14] prepared Si_3N_4/TiN ceramic composite using reaction sintering of Si_3N_4/TiO_2 powder mixtures. Ling *et al.* [15] prepared TiC/Si_3N_4 composites using Si_3N_4 powder by self-propagating high temperature synthesis and TiC spark plasma sintering. Tian *et al.* [16] have reported thermal shock and thermal fatigue behaviours of Si_3N_4 and Si_3N_4-TiC ceramics. They reported that TiC-Si_3N_4 ceramics exhibit higher residual strength compared to Si_3N_4 ceramics. Zhao *et al.* [17] synthesized nano-sized Si_3N_4/TiC composites and they reported that mechanical properties were improved for the composite with the addition of 10 wt.% Si_3N_4 nanoparticles and 15 wt.% TiC nanoparticles. Gao *et al.* [18] prepared TiN-Si_3N_4 ceramics and found that the addition of 20 vol.% of TiN increases the bending strength of the composite to 1154 MPa. Based on these facts, literature survey was conducted and it was observed that there are not many reports based on DFT method to study the mechanical properties of Si_3N_4 based ceramics. The DFT method gives insights on an atomistic level in Si_3N_4 based ceramics. The elastic constants, electronic properties and stress-strain variation, fracture toughness and Pugh's criteria of β-Si_3N_4 nanostructures, TiC-Si_3N_4 and TiN-Si_3N_4 ceramics are studied and reported.

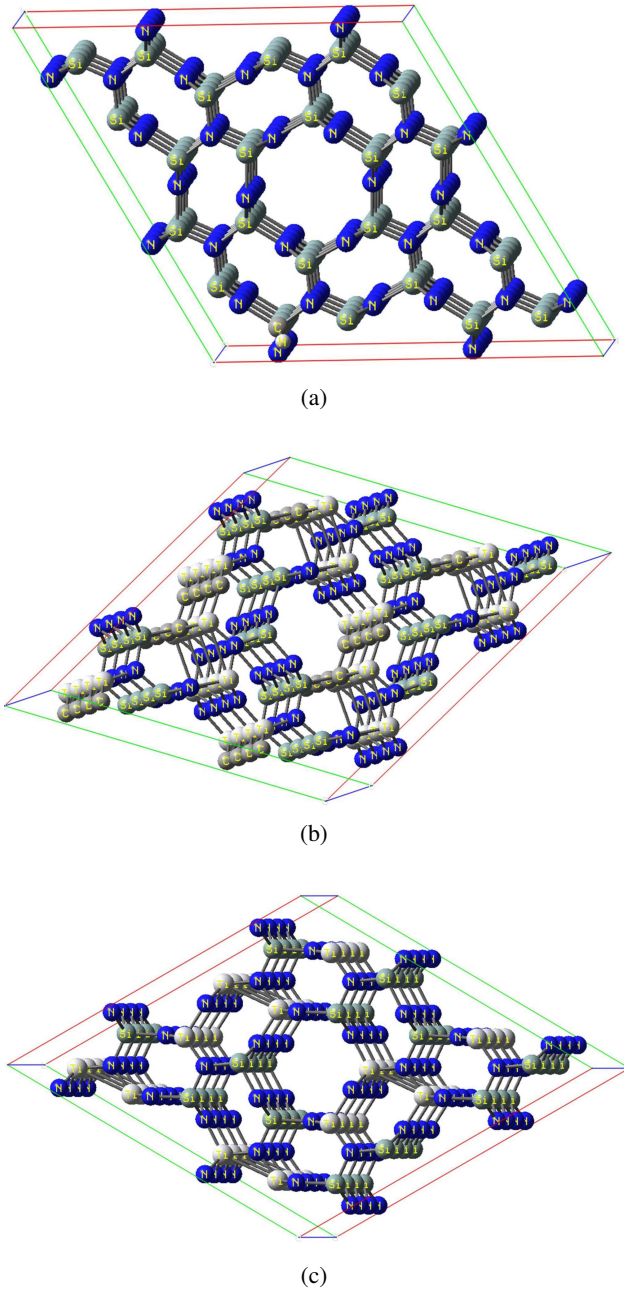

(a)

(b)

(c)

Figure 1. Structure of: a) pristine β-Si_3N_4, b) TiC-Si_3N_4 and c) TiN-Si_3N_4 ceramics

II. Computational details

The mechanical properties of β-Si_3N_4 nanostructures, TiC-Si_3N_4 and TiN-Si_3N_4 ceramics are studied using DFT method utilizing TranSIESTA module in SIESTA package [19]. Optimization of β-Si_3N_4 nanostructures is carried out using pseudo potentials in SIESTA code. The β-Si_3N_4 nanostructures are modelled by decreasing the atomic forces on the atoms to be lesser than 0.05 eV/Å. The generalized gradient approximation (GGA) combined with Perdew-Burke-Ernzerhof (PBE) exchange correlation functional is utilized to investigate the electron-electron interaction [20,21]. The Brillouin zones are sampled using Monkhorst-Pack scheme with 8×8×8 mesh for calculations. The stress-strain characteristics of β-Si_3N_4 are also studied with SIESTA package, in which the core electrons are substituted, suitably by Troullier-Martins pseudo potentials for titanium and oxygen atoms. The wave function of silicon, nitrogen, titanium, carbon and nitrogen atoms are expanded in terms of double zeta polarization (DZP) [22] basis set, which mainly depends on the numerical orbitals.

III. Results and discussion

3.1. Calculation of elastic constants

The computation of elastic constants is calculated from the change in energy with the influence of small strains to the equilibrium β-Si_3N_4 lattice configuration. The elastic energy of β-Si_3N_4 nanostructure under the application of strain is given as:

$$\frac{\Delta E}{V} = \frac{1}{2}\sum_{i=1}^{6}\sum_{j=1}^{6} C_{ij}\cdot e_i \cdot e_j \qquad (1)$$

where ΔE is the change in energy of the unit cell on application of strain vector given by $e = (e_1, e_2, e_3, e_4, e_5, e_6)$, V is the equilibrium volume of unstrained lattice; C is the elastic constant of matrix.

For hexagonal phases, there are five linearly independent elastic constants, $C_{11}, C_{12}, C_{13}, C_{33}, C_{44}$ and C_{55} [23,24]. The sixth elastic constant, C_{66} is the linear combination of both C_{11} and C_{12}:

$$C_{66} = \frac{1}{2}(C_{11} - C_{12}) \tag{2}$$

The hexagonal phase of β-Si_3N_4 has two lattice parameters a and c along with matrix form of Bravais lattice vectors given by:

$$R = \begin{pmatrix} \frac{\sqrt{3}}{2}a & -\frac{1}{2}a & 0 \\ -\frac{\sqrt{3}}{2}a & \frac{1}{2}a & 0 \\ 0 & 0 & \frac{c}{a} \end{pmatrix} \tag{3}$$

k-points grid utilized in this case is 8×8×8 with cut-off energy of 500 eV. R is referred to strain according to the equation $R' = R \cdot D$ where D is the distortion matrix and R' is the deformed matrix with respect to distorted lattice vectors. Thus, there are five possible strains, which is to be applied and five independent elastic constants, namely $C_{11}, C_{12}, C_{13}, C_{33}$ and C_{44}, are calculated. The distortion matrices $D1$–$D5$ with corresponding strain energy are expressed in equation 4–13, respectively.

$$D1 = \begin{pmatrix} 1+\delta & 0 & 0 \\ 0 & 1+\delta & 0 \\ 0 & 0 & 1+\delta \end{pmatrix} \tag{4}$$

where the c/a ratio is considered to be a constant due to the small lattice distortion introduced by the expansion or compression to the system. In this case, volume changes but the symmetry is conserved. The corresponding strain energy of this distortion $D1$ is:

$$E(V,\delta) = E(V_0,0) + V_0\Big[(\tau_1+\tau_2+\tau_3)\delta + \\ + \frac{1}{2}(2C_{11}+2C_{12}+4C_{13}+C_{33})\delta^2\Big] \tag{5}$$

The distortion $D2$ conserves both symmetry and volume:

$$D2 = \begin{pmatrix} (1+\delta)^{-1/3} & 0 & 0 \\ 0 & (1+\delta)^{-1/3} & 0 \\ 0 & 0 & (1+\delta)^{-1/3} \end{pmatrix} \tag{6}$$

$$E(V,\delta) = E(V_0,0) + V_0\Big[(\tau_1+\tau_2+\tau_3)\delta + \\ + \frac{1}{9}(C_{11}+C_{12}-4C_{13}+2C_{33})\delta^2\Big] \tag{7}$$

The distortion matrix $D3$ compresses the cell along axis-b and elongates along axis-a while conserving volume:

$$D3 = \begin{pmatrix} \frac{1+\delta}{(1-\delta)^{1/3}} & 0 & 0 \\ 0 & \frac{1-\delta}{(1-\delta)^{1/3}} & 0 \\ 0 & 0 & \frac{1}{(1-\delta)^{1/3}} \end{pmatrix} \tag{8}$$

$$E(V,\delta) = E(V_0,0) + V_0\Big[(\tau_1-\tau_2)\delta + \frac{1}{9}(C_{11}-C_{12})\delta^2\Big] \tag{9}$$

C_{55} can be found with the distortion matrix $D4$ with conserved volume:

$$D4 = \begin{pmatrix} \frac{1}{(1-\delta)^{1/3}} & 0 & \frac{\delta}{(1-\delta)^{1/3}} \\ 0 & \frac{1}{(1-\delta)^{1/3}} & 0 \\ \frac{\delta}{(1-\delta)^{1/3}} & 0 & \frac{1}{(1-\delta)^{1/3}} \end{pmatrix} \tag{10}$$

$$E(V,\delta) = E(V,0) + V_0\left(\tau_5\delta + 2C_{55}\delta^2\right) \tag{11}$$

The distortion matrix $D5$ compressed or stretched along the axis-c, while keeping the axis a and b unchanged:

$$D5 = \begin{pmatrix} 1 & 0 & 0 \\ 0 & 1 & 0 \\ 0 & 0 & 1+\delta \end{pmatrix} \tag{12}$$

$$E(V,\delta) = E(V,0) + V_0\left(\tau_3\delta + \frac{1}{2}C_{33}\delta^2\right) \tag{13}$$

3.2. Calculation of mechanical properties

Shear modulus of β-Si_3N_4 nanostructures, TiC-Si_3N_4 and TiN-Si_3N_4 ceramics are calculated from Voigt (V), Reuss (R) and Hill's (H) analysis [25], which is given as:

$$B_V = \frac{2}{9}\left(C_{11}+C_{12}+2C_{13}+\frac{C_{33}}{2}\right) \tag{14}$$

$$B_R = \frac{(C_{11}+C_{12})\cdot C_{33} - 2C_{13}^2}{C_{11}+C_{12}+2C_{33}-4C_{13}} \tag{15}$$

$$G_V = \frac{C_{11}+C_{12}+2C_{33}-4C_{13}+12C_{44}+12C_{66}}{30} \tag{16}$$

$$G_R = \frac{\frac{5}{2}AC_{44}C_{66}}{3B_VC_{44}C_{66}+A(C_{44}+C_{66})} \tag{17}$$

where $A = (C_{11}+C_{12})C_{33} - 2C_{13}^2$.

$$G_H = \frac{G_V+G_R}{2} \tag{18}$$

$$B_H = \frac{B_V+B_R}{2} \tag{19}$$

$$\sigma = \frac{3B_H-2G_H}{2(3B_H+G_H)} \tag{20}$$

$$Y = \frac{9B_H G_H}{3B_H + G_H} \tag{21}$$

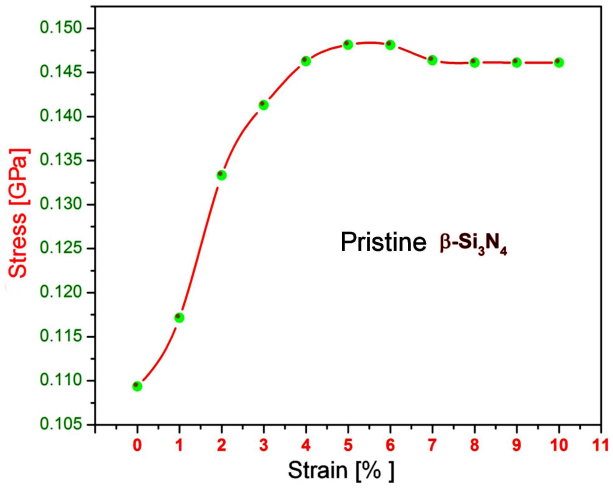

(a)

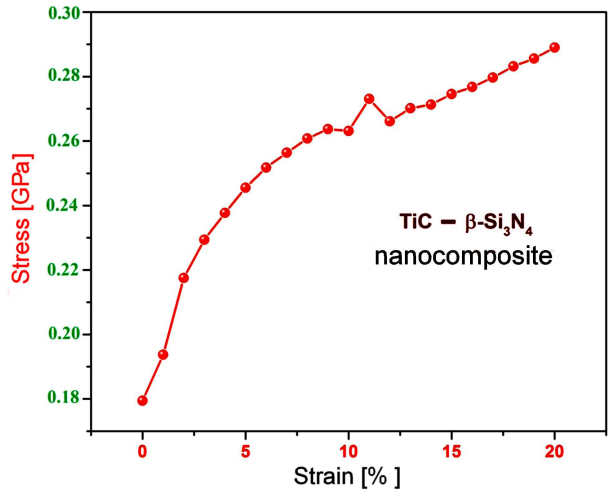

(b)

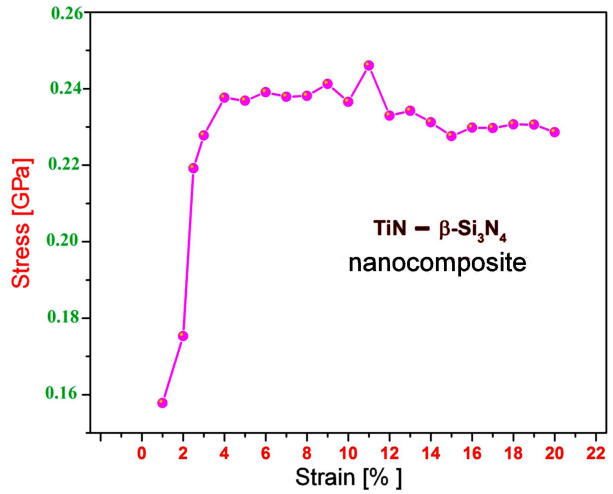

(c)

Figure 2. Stress-strain curve of: a) pristine β-Si_3N_4, b) TiC-Si_3N_4 and c) TiN-Si_3N_4 ceramics

where G_V, G_H, G_R, B_V, B_H and B_R are the Voigt's shear modulus, Hill's shear modulus, Reuss's shear modulus, Voigt's bulk modulus, Hill's bulk modulus and Reuss's bulk modulus, respectively [26] and σ is the Poisson's ratio of β-Si_3N_4 nanostructures. In the present work, the mass ratio between the secondary phase (TiC and TiN) and Si_3N_4 was 35.71 to 64.29.

3.3. Stress-strain curve

The stress-strain characteristics of the pristine β-Si_3N_4 nanostructures, TiC-Si_3N_4 and TiN-Si_3N_4 ceramics are studied in order to explore the mechanical properties. Figure 1 represents structure of the pristine β-Si_3N_4 nanostructures, TiC-Si_3N_4 and TiN-Si_3N_4 ceramics. The strain along the length of the hexagonal lattice is increased in steps of 1%. During the relaxation process, the application of strain along the z direction results in significant change in stress along zz direction. When the pristine β-Si_3N_4 nanostructure is subjected to the tensile test it undergoes various stages, which is shown in the stress-strain curve. Moreover, the analysis of the stress-strain curve becomes crucial to ascertain the strength and fracture toughness [27] of β-Si_3N_4 ceramics. Figure 2 illustrates the stress-strain curve of β-Si_3N_4, TiC-Si_3N_4 and TiN-Si_3N_4 ceramics. In the stress-strain characteristics curve of the pristine β-Si_3N_4 nanostructures, a linear elongation along z direction is observed, which obeys Hooke's law until the strain of 2%. Beyond 2% strain, the stress increases steadily for applied strain up to 6.5%. Further application of strain, gives rise to necking and creep formation takes place with a decrease in stress. Moreover, the fracture point is observed for the strain of 10% and the pristine β-Si_3N_4 nanostructures are permanently deformed [28]. Furthermore, in the case of TiC-Si_3N_4 ceramics, the fluctuation in the stress-strain curve is observed at a strain of 10% (Fig. 2b). The fluctuation in stress-strain behaviour is attributed to the slipping between the layers and the formation of Lüder's bands [29]. After the formation of the Lüder's bands, there is an increase in the value of stress, for the applied strain untill 20%. Beyond 20% strain, TiC-Si_3N_4 ceramics get fractured. The super plasticity exhibited by TiC-Si_3N_4 ceramics is due to the fact that 35.71 wt.% of TiC is present in the composite, which leads to an alignment of nanostructure in the direction of tensile stress. However, the formation of TiC-Si_3N_4 nanostructures leads to the increase in the fracture limit up to 20%.

From the stress-strain curve of TiN-Si_3N_4 ceramics, it is inferred that the elastic region is minimized compared to TiC-Si_3N_4 ceramics. As a result, proof resilience is lower than TiC-Si_3N_4 ceramics and is harder in nature. Once the elastic limit is reached, many fluctuations in stress-strain behaviour are observed in the case of TiN-Si_3N_4 ceramics, which is due to the similar reason, i.e. formation of Lüder's bands as quoted in TiC-Si_3N_4 ceramics. The formation of peak in the curve is observed when the strain applied is between 0.1–0.12, which can

Table 1. Elastic tensors of pristine β-Si_3N_4, TiC-Si_3N_4 and TiN-Si_3N_4 ceramics

Nanostructures	C_{11}	C_{12}	C_{13}	C_{33}	C_{44}	C_{66}
β-Si_3N_4 nanostructure	394.89	265.52	251.18	177.65	232.76	333.51
TiC-Si_3N_4 ceramics	401.01	275.56	252.591	383.447	260.77	356.51
TiN-Si_3N_4 ceramics	437.47	396.36	336.61	551.119	308.43	395.63

Table 2. Bulk modulus (B), Young's modulus (Y), shear modulus (G), Poisson's ratio (σ), B/G ratio of β-Si_3N_4, TiC-Si_3N_4 and TiN-Si_3N_4 ceramics

Material	B [GPa]	Y [GPa]	G [GPa]	σ	B/G ratio	Yield point	Break point
β-Si_3N_4 nanostructure	122.80	409.88	217.15	0.056	0.566	4%	10%
TiC-Si_3N_4 ceramics	125.90	456.51	254.84	0.104	0.494	9%	20%
TiN-Si_3N_4 ceramics	130.13	482.88	273.88	0.118	0.475	4%	20%

be inferred as the ultimate tensile strength. Beyond that the creep formation occurs, where the material fails permanently when the strain is above 0.2. Thus, it is evident from the stress-strain characteristics that β-Si_3N_4 and its composites get deformed only after large strain. This is due to the formation of large inter-granular glass pockets [27], which improves tribological properties. It is also inferred that the elastic limit of TiN-Si_3N_4 ceramics is lower than that of TiC-Si_3N_4 ceramics, which implies that TiN-Si_3N_4 ceramics is less ductile but harder. Also the stress corresponding to the applied strain is higher in the case of TiN-Si_3N_4 ceramics, which indicates that TiN-Si_3N_4 ceramics is tougher and has a higher modulus of elasticity compared with TiC-Si_3N_4 ceramics, which is evident from the computed results.

Elastic constant plays a vital role in investigating the mechanical properties of the material. Table 1 represents the elastic tensors of the pristine β-Si_3N_4, TiC-Si_3N_4 and TiN-Si_3N_4 ceramics. In general Hooke's law is given by $\sigma_{ij} = \varepsilon \cdot C_{ijkl}$, where σ_{ij} is the stress tensor, C is the matrix of elastic constants and ε is strain tensor. The symmetry of Cauchy's stress tensor shows that $\sigma_{ij} = \sigma_{ji}$ $(i, j = 1, 2, 3, 4, 5, 6)$ are the minor symmetry and the major symmetry of the infinitesimal strain tensor implying that $C_{ijkl} = C_{ijlk}$ $(i, j, k, l = 1, 2, 3)$.

Table 2 depicts the bulk modulus, Young's modulus, shear modulus, Poisson's ratio, B/G ratio of β-Si_3N_4, TiC-Si_3N_4 and TiN-Si_3N_4 ceramics, respectively. It is observed that the values of bulk modulus follow the order TiN-Si_3N_4 > TiC-Si_3N_4 > β-Si_3N_4. The result indicates that TiN-Si_3N_4 ceramics are less compressible in nature. The value of Young's modulus determines the ability of the material to elongate, which implies that β-Si_3N_4 is more elastic in nature. In the case of TiC-Si_3N_4 and TiN-Si_3N_4 ceramics, the bonding of Ti, C and N with Si and N, results in decrease of Young's modulus. Shear modulus indicates the tendency of the planes to slip over each other and from the observations, it is inferred that β-Si_3N_4 is more suitable for torsional applications, such as propeller shafts. In addition, the B/G ratio of β-Si_3N_4, TiC-Si_3N_4 and TiN-Si_3N_4 ceramics gives the quantitative measurement of the ductility of the material, which follows the order TiN-Si_3N_4 < TiC-Si_3N_4 < β-Si_3N_4, which is based on Pugh's criteria [25]. Moreover, the crack propagation starts from the surface of the material and it is mandatory to estimate the fracture toughness of the material. From the study it is known that the fracture toughness of β-Si_3N_4 is observed to be 6.70 MPa·$m^{1/2}$, which is in close agreement with the values reported [30]. Hence it exhibits high resistance to crack formation. Besides, TiC-Si_3N_4 exhibits enhanced fracture toughness of 19.10 MPa·$m^{1/2}$, bulk modulus, thermal stability and tribological property, which can be used for bearings and turbine blades. Furthermore, TiN-Si_3N_4 ceramics have high hardness, porosity, high fracture toughness of 25.55 MPa·$m^{1/2}$ and excellent surface properties that can be used for gears and shafts [31]. The order of fracture toughness is found to be TiN-Si_3N_4 > TiC-Si_3N_4 > β-Si_3N_4. Moreover, Si_3N_4 based ceramics are the material with high value of bulk modulus and resilience and therefore it can be used in orthopaedic implants [32].

3.4. Band structures

The band structure of β-Si_3N_4, TiC-Si_3N_4 and TiN-Si_3N_4 ceramics gives the insight on the material properties of these nanostructures. Figure 3 illustrates the band structure of the pristine β-Si_3N_4, TiC-Si_3N_4 and TiN-Si_3N_4 ceramics. It is inferred that the band gap along the gamma point G is found to be 3.96 eV for the pristine β-Si_3N_4 nanostructure. However, the experimental energy gap value of Si_3N_4 varies from 2.43 to 4.74 eV [33]. Moreover, DFT study underestimates the band gap, since DFT method is applicable for ground state configuration. In the present work, the band gap of 3.96 eV for the pristine β-Si_3N_4 nanostructures represents the insulating nature of nanostructure. However, in the case of TiC-Si_3N_4 ceramics the band gap is calculated to be 2.22 eV. The bonding of TiC with Si_3N_4 modifies the band gap. Since the electronic configuration of Ti and C are [Ar] $3d^2\,4s^2$, [He] $2s^2\,2p^2$, respectively, the orbital overlapping leads to decrease in the band gap of TiC-Si_3N_4 ceramics. In the case of TiN-Si_3N_4 ceramics, the band gap is observed to be around 2.64 eV. Since the electronic configuration of N is $1s^2\,2s^2\,2p^3$, the orbital overlapping results in the decrease in the band gap compared with the pristine counterpart. The electronic properties are influenced by the charge trapping centres,

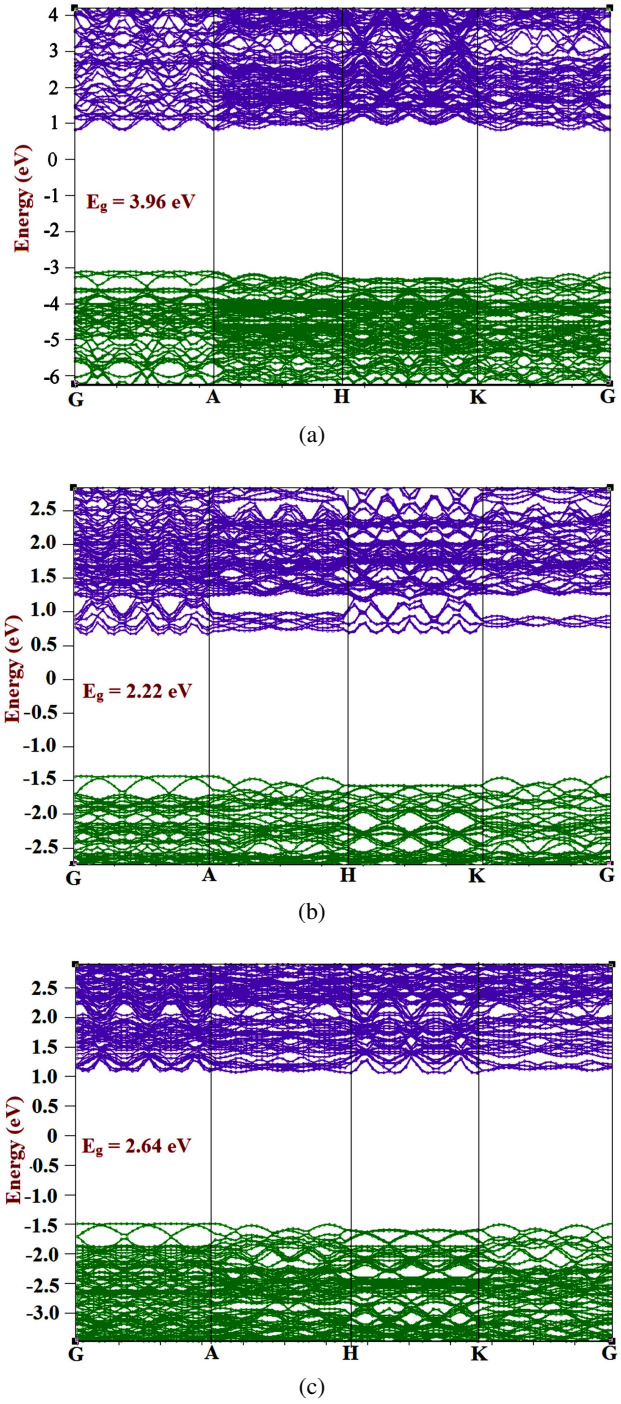

Figure 3. Band structure of: a) pristine β-Si_3N_4, b) TiC-Si_3N_4 and c) TiN-Si_3N_4 ceramics

the presence of Si and N dangling bonds also have influence in the band structure, which appears in the amorphous matrix of silicon nitride. Furthermore, the presence of TiC and TiN in β-Si_3N_4 ceramics leads to altered properties in terms of electronic properties. The band structure plays an important role in the property of gate dielectric in thin film based transistors as well as in charge storage medium in nonvolatile memory [34]. From the observations, it is inferred that the band gap can be fine-tuned in Si_3N_4 nanostructures upon incorporation of TiC or TiN in Si_3N_4-based ceramics.

3.5. Density of states

The atomic orbital population gives the perception on the distribution of electrons along *s*, *p* and *d* orbits, which is illustrated in terms of total density of states (TDOS) spectrum [35,36]. The total value is the sum of the valence electrons in each atom in β-Si_3N_4 nanostructure, TiC-Si_3N_4 and TiN-Si_3N_4 ceramics. The major contribution for the pristine β-Si_3N_4 arises from the contribution of Si $3p$ with N $2p$ states. Moreover, the orbital overlapping due to the bonding of silicon with the nitrogen atom shows more peak maxima in the valence band in the range of −5 to −25 eV. The peak maxima are observed in the conduction band from 0 to 10 eV. However, in the case of TiC-Si_3N_4 ceramics, the overlapping of $3d$ and $4s$ orbitals in Ti and C atoms with Si $3p$ and N $2p$ orbitals gives rise to increased number of peak maxima in the valence band and in the conduction band. The decrease in the band gap for TiC-Si_3N_4 ceramics is due to the orbital overlapping, which is also observed in TDOS spectrum of TiC-Si_3N_4 ceramics. In addition, the excess of electron in nitrogen atom of TiN gives rise to more peak maxima in TiN-Si_3N_4 ceramics. The peak maxima are observed in the energy range of −5 to −25 eV along the valence band. From TDOS spectrum, more number of peak maxima in the valence band and in the conduction band of TiN-Si_3N_4 is observed; it confirms the decrease of band gap compared to the pristine Si_3N_4 nanostructure. In the case of β-Si_3N_4, which is found to be most stable, the nitrogen atoms form bonds with first three Si neighbouring atoms in the planar structure forming sp^2 hybridization. Moreover, the Si atoms form bond with the first four neighbours in the tetrahedral structure by sp^3 hybridization. However, the presence of TiC and TiN in β-Si_3N_4 ceramics modifies the hybridization, which gives rise to shift in the peak maxima. The high melting temperature, chemical inertness, strong resistance against thermal shock, high dielectric constant arise to the density of states in β-Si_3N_4 nanostructures. In summary, TDOS spectrum indicates that the density of states of Si_3N_4 nanostructures can be fine-tuned with the incorporation of impurities in β-Si_3N_4 nanostructure. Figure 4 represents the TDOS spectrum of β-Si_3N_4, TiC-Si_3N_4 and TiN-Si_3N_4 ceramics.

IV. Conclusions

The mechanical and electronic properties of β-Si_3N_4 nanostructures, TiC-Si_3N_4 and TiN-Si_3N_4 ceramics are studied using DFT method in combination with GGA/PBE functional. For the pristine β-Si_3N_4 nanostructures, the fracture point is observed for a strain of 10%. TiC-Si_3N_4 ceramics exhibits fluctuation in stress-strain curve, beyond 20% TiC-Si_3N_4 ceramics fractures. Besides, TiN-Si_3N_4 are observed to be harder and less ductile than the pristine and TiC-Si_3N_4 ceramics. The bulk modulus is found to be in the order TiN-Si_3N_4 > TiC-Si_3N_4 > β-Si_3N_4. Furthermore, it can be concluded

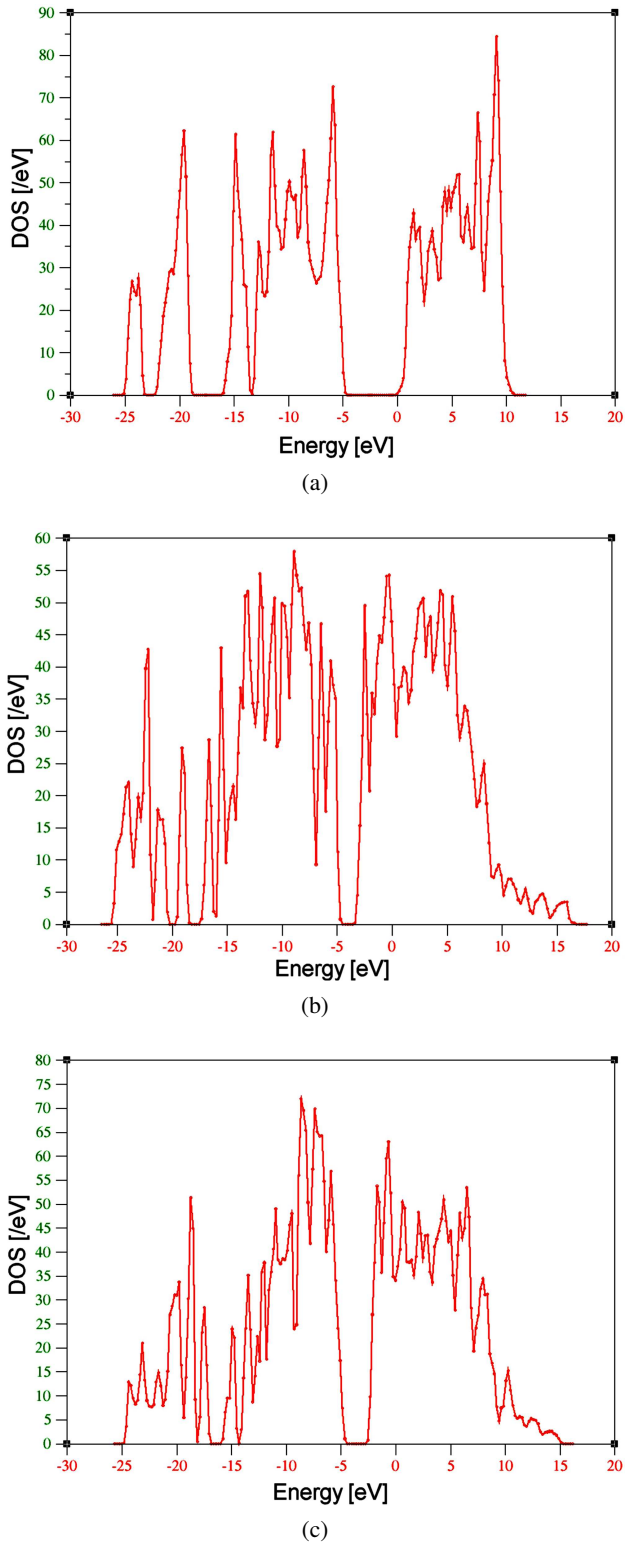

Figure 4. Density of states spectrum of: a) pristine β-Si_3N_4, b) TiC-Si_3N_4 and c) TiN-Si_3N_4 ceramics

that TiN-Si_3N_4 is the least compressible in nature. The band structure studies show that the band gap of β-Si_3N_4 nanostructures is observed to be higher than TiC-Si_3N_4 and TiN-Si_3N_4 ceramics. It is inferred that the band gap can be tailored using suitable impurities in β-Si_3N_4 nanostructures. The TDOS spectrum shows more peak maxima for TiC-Si_3N_4 and TiN-Si_3N_4 than the pristine β-Si_3N_4. From the results of TDOS spectrum, it can be concluded that β-Si_3N_4 nanostructures can be fine-tuned with composites. The finding of the present study gives an insight on the mechanical and electronic properties of the pristine β -Si_3N_4, TiC-Si_3N_4 and TiN-Si_3N_4 ceramics.

References

1. L. Cui, M. Hu, Q. Wang, B. Xu, D. Yu, Z. Liu, J. He, "Prediction of novel hard phases of Si_3N_4: First-principles calculations", *J. Solid State Chem.*, **228** (2015) 20–26.
2. C. Dong, Y. Ben-Hai, "Pressure-induced phase transition in silicon nitride material", *Chinese Phys. B.*, **22** (2013) 23104.
3. K. Chen, Z. Huang, Y.G. Liu, M. Fang, J. Huang, Y. Xu, "Synthesis of β-Si_3N_4 powder from quartz via carbothermal reduction nitridation", *Powder Technol.*, **235** (2013) 728–734.
4. W.-C. Lee, S.-L. Chung, "Combustion synthesis of Si_3N_4 powder", *J. Mater. Res.*, **12** (1997) 805–811.
5. H.L. Zhu, F.D. Han, J.Q. Bi, Y.J. Bai, Y.X. Qi, L.L. Pang, C.G. Wang, S.J. Li, C.W. Lu, "Facile synthesis of Si_3N_4 nanocrystals via an organic-inorganic reaction route", *J. Am. Ceram. Soc.*, **92** (2009) 535–538.
6. Y. Xia, Y.P. Zeng, D. Jiang, "Dielectric and mechanical properties of porous Si_3N_4 ceramics prepared via low temperature sintering", *Ceram. Int.*, **35** (2009) 1699–1703.
7. X. Fu, N. Zhu, Z. Peng, "One-step synthesis and characterization of tree-like branched α-Si_3N_4 nano/submicron-structures by pyrolysis of a polymer precursor", *Solid State Sci.*, **14** (2012) 1267–1272.
8. A. Kalemtas, G. Topates, H. Özcoban, H. Mandal, F. Kara, R. Janssen, "Mechanical characterization of highly porous β-Si_3N_4 ceramics fabricated via partial sintering & starch addition", *J. Eur. Ceram. Soc.*, **33** (2013) 1507–1515.
9. G. Blugan, M. Hadad, T. Graule, J. Kuebler, "Si_3N_4-TiN-SiC three particle phase composites for wear applications", *Ceram. Int.*, **40** (2014) 1439–1446.
10. J. Wu, Y. Zhang, X. Xu, X. Lao, K. Li, X. Xu, "A novel in-situ β-Sialon/Si_3N_4 ceramic used for solar heat absorber", *Ceram. Int.*, **41** (2015) 14440–14446.
11. Y. Xing, J. Deng, K. Zhang, X. Wang, Y. Lian, Y. Zhou, "Fabrication and dry cutting performance of S_3N_4/TiC ceramic tools reinforced with the PVD WS/Zr soft-coatings", *Ceram. Int.*, **41** (2015) 10261–10271.
12. R.G. Duan, G. Roebben, J. Vleugels, O. Vanderbiest, "Effect of TiX (X = C, N, O) additives on microstructure and properties of silicon nitride based ceramics", *Scr. Mater.*, **53** (2005) 669–673.
13. Y.F. Kargin, S.N. Ivicheva, A.S. Lysenkov, N.A. Ovsyannikov, L.I. Shvorneva, K.A. Solntsev, "Si_3N_4/TiN composites produced from TiO_2-modified Si_3N_4 powders", *Inorg. Mater.*, **48** (2012)

897–902.
14. A. Maglica, K. Krnel, T. Kosmac, "Prepararion of Si_3N_4-TiN ceramic composites", *Mater. Technol.*, **44** (2010) 31–35.
15. L. Bai, C. Ge, W. Shen, X. Mao, K. Zhang, "Densification, microstructure, and fracture behavior of TiC/Si_3N_4 composites by spark plasma sintering", *Rare Met.*, **27** (2008) 315–319.
16. C. Tian, N. Liu, M. Lu, "Thermal shock and thermal fatigue behavior of Si_3N_4-TiC nano-composites", *Int. J. Refract. Met. Hard Mater.*, **26** (2008) 478–484.
17. J. Zhao, X. Ai, Z. Lu, "Preparation and characterization of Si_3N_4/TiC nanocomposite ceramics", *Mater. Lett.*, **60** (2006) 2810–2813.
18. L. Gao, J. Li, T. Kusunose, K. Niihara, "Preparation and properties of TiN-Si_3N_4 composites", *J. Eur. Ceram. Soc.*, **24** (2004) 381–386.
19. J.M. Soler, E. Artacho, J.D. Gale, A. Garcìa, J. Junquera, P. Ordejòn, D. Sanchez-Portal, "SIESTA method for ab initio order-N materials simulation", *J. Phys. Condens. Matter*, **14** (2002) 2745–2779.
20. J. Perdew, K. Burke, Y. Wang, "Generalized gradient approximation for the exchange-correlation hole of a many-electron system", *Phys. Rev. B.*, **54** (1996) 16533–16539.
21. J. Perdew, J. Chevary, S. Vosko, K. Jackson, M. Pederson, D. Singh, C. Fiolhais, "Atoms, molecules, solids, and surfaces: Applications of the generalized gradient approximation for exchange and correlation", *Phys. Rev. B.*, **46** (1992) 6671–6687.
22. S. Sriram, V. Nagarajan, R. Chandiramouli, "H_2S and NH_3 adsorption characteristics on CoO nanowire molecular device – A first-principles study", *Chem. Phys. Lett.*, **636** (2015) 51–57.
23. P. Ravindran, P. Vajeeston, R. Vidya, A. Kjekshus, H. Fjellvåg, "Detailed electronic structure studies on superconducting MgB_2 and related compounds", *Phys. Rev. B*, **64** (2001) 224509.
24. L. Fast, J.M. Wills, B. Johansson, O. Eriksson, "Elastic constants of hexagonal transition metals: Theory", *Phys. Rev. B*, **51** (1995) 17431.
25. C.M. Li, S.M. Zeng, Z.Q. Chen, N.P. Cheng, T.X. Chen, "First-principles calculations of elastic and thermodynamic properties of the four main intermetallic phases in Al-Zn-Mg-Cu alloys", *Comput. Mater. Sci.*, **93** (2014) 210–220.
26. C. Jiang, Z. Lin, Y. Zhao, "Thermodynamic and mechanical stabilities of tantalum nitride", *Phys. Rev. Lett.*, **103** (2009) 185501.
27. H.-J. Kleebe, G. Pezzotti, G. Ziegler, "Microstructure and fracture toughness of Si_3N_4 ceramics: Combined roles of grain morphology and secondary phase chemistry", *J. Am. Ceram. Soc.*, **82** [7] (1999) 1857–1867.
28. G.A. Gogotsi, "Mechanical behaviour of a silicon nitride particulate ceramic composite", *Ceram. Int.*, **35** (2009) 1109–1114.
29. F. Garofalo, "Comments on the internal stress during the propagation of Luder's bands in iron", *Mater. Sci. Eng.*, **16** (1974) 291–293.
30. M. Turon-Vinas, M. Anglada, "Assessment in Si_3N_4 of a new method for determining the fracture toughness from a surface notch micro-machined by ultrashort pulsed laser ablation", *J. Eur. Ceram. Soc.*, **35** (2015) 1737–1741.
31. J. Huang, P.K. Nayak, "Effect of nano-TiN on mechanical behavior of Si_3N_4 based nanocomposites by spark plasma sintering (SPS)", pp. 421–436 in *Nanocomposites – New Trends and Developments*. Ed. F. Ebrahimi, InTech, Croatia, 2012.
32. M. Mazzocchi, A. Bellosi, "On the possibility of silicon nitride as a ceramic for structural orthopaedic implants. Part I: Processing, microstructure, mechanical properties, cytotoxicity", *J. Mater. Sci.: Mater. Med.*, **19** (2008) 2881–2887.
33. S.V. Deshpande, E. Gulari, S.W. Brown, S.C. Rand, "Optical properties of silicon nitride films deposited by hot filament chemical vapor deposition", *J. Appl. Phys.*, **77** (1995) 6534.
34. F. De Brito Mota, J. F. Justo, A. Fazzio, "Structural and electronic properties of silicon nitride materials", *Int. J. Quantum Chem.*, **70** (1998) 973–980.
35. R. Chandiramouli, V. Nagarajan, "Tuning band structure and electronic transport properties of ZrN nanotube – A first-principles investigation", *Spectrochim. Acta, Part A*, **136** (2015) 1018–1026.
36. V. Nagarajan, V. Saravanakannan, R. Chandiramouli, "DFT investigation on structural stability and electronic properties of α-Si_3N_4 and β-Si_3N_4 nanostructures", *Int. J. Chem. Tech. Res.*, **6** (2014) 5466–5475.